Volume 1 | Number 1 | Jan 2013 | Pages 1–100

PCCP

Physical Chemistry Chemical Physics
www.rsc.org/pccp

ROYAL SOCIETY OF CHEMISTRY

ROYAL SOCIETY OF CHEMISTRY

www.rsc.org/pccp

Journal Name

ARTICLE

Morphological and structural evolution of WS$_2$ nanosheets irradiated with an electron beam

Yuqing Wang, Yi Feng*, Yangming Chen, Fei Mo, Gang qian, Dongbo Yu, Yang Wang and Xuebin Zhang

The morphological and structural evolution of WS$_2$ nanosheets under electron irradiation are investigated using high-resolution transmission electron microscopy. During irradiation, the sulfur atoms that interacted with the electrons were sputtered first and the tungsten atoms began to sputter when the surrounding sulfur atoms had been sputtered. With an increasing irradiation time, the remaining tungsten atoms rearranged to form new structures. In addition, the damage to the WS$_2$ nanosheets became more severe with increasing electron energies and irradiation times.

Introduction

Currently, transition metal dichalcogenides (TMDs) with the common structural formula AB$_2$, where A stands for transition metals (such as Mo, W and Ti) and B for chalcogens (such as S, Se and Te), are receiving a significant amount of attention. In particular, TMDs have a wide range of applications owing to their unique structure where a layer of A atoms is sandwiched between two layers of B atoms (B-A-B layer).[1] The atoms in each layer are held together strongly by covalent bonds, while the interlayers are weakly held together by van der Waals forces. What is more, TMDs also have versatile electronic structures, varying from metallic to semiconducting behavior.[2,3] Among many of the reported TMDs, MoS$_2$ and WS$_2$ have been extensively studied. They have been studied as high-temperature lubricants, as well as intercalation materials in rechargeable batteries. It is only recently that the focus has shifted to single layer or few-layer nanosheets of MoS$_2$ and WS$_2$. The effective methods used to synthesize MoS$_2$ and WS$_2$ nanosheets are sonication[4-6] and ion intercalation[7-9]. TMDs have special structures, which enable them to be used in single-layer transistors,[10,11] rechargeable batteries[12-14] and optoelectronic devices.[15-17] WS$_2$ has also been used as a solid lubricant in aerospace. In addition, R. Bhandavat *et al* synthetized surface-functionalized WS$_2$ nanosheets and studied their performance as Li-ion battery anodes.[18]

Recently, unprecedented levels of imaging contrast and resolution have become available owing to advances in high-resolution transmission electron microscopy (HRTEM).[19-21] Many useful materials have been studied using HRTEM, which have been used in many studies to characterize TMDs materials with atomic resolution. HRTEM observes the dynamics of individual atoms under the controlled influence of electron beams, allowing this method to have the potential to provide an instrument to measure chemical constants, cross sections of the damage events and other characteristics of the dynamic processes that occur on the atomic scale.[22]

Incontrovertibly, more and more devices using TMDs are often required to work in a radiation-hostile environment such as in space applications, nuclear reactors, and scientific instruments. Therefore, a good understanding of the radiation damage to these materials is important for these different fields. However, very few have studied the effects of electron irradiation on WS$_2$ nanosheets. Jacopo Brivio *et al.* observed the electron irradiation of ultrathin MoS$_2$ membranes[23] and the defects in monolayer MoS$_2$ under electron irradiation.[24] They used HRTEM to observe the production of defects in the atomic structures, because not only does HRTEM create defects in a controllable manner, it also monitors the variations in situ. In this paper, HRTEM is used both as an irradiation source and to study the in-situ morphological and structural changes in WS$_2$ nanosheets under the irradiation of an electron beam. The effects of electron irradiation on WS$_2$ nanosheets are also studied, because the irradiation damage mechanism present in WS$_2$ nanosheets can be extended to other WS$_2$-based materials and TMDs. It is believed that studying irradiated WS$_2$ nanosheets will provide useful informations for the selection of materials that must undergo irradiation either during or prior to application.

Experimental

To prepare the HRTEM (JEM-2100F) samples, WS$_2$ nanosheets (purchased from Nanjing XFNANO Materials Tech Co., Ltd., China) were dispersed in ethanol and ultrasonicated for 30 min. The mixed solution was then dropped onto a Cu grid. The HRTEM images were carried out at electron acceleration voltages of 100, 120 and 200 kV with a current density of 1.0×10^5 Acm^{-2} and a single frame acquisition time of 1 s. Before the HRTEM measurements, liquid nitrogen was poured into the reservoir to lower the temperature at 41.15K. Moreover, the effect of irradiation was reduced at a negligible level when images were taken to guarantee the image quality.[25]

Results and discussion
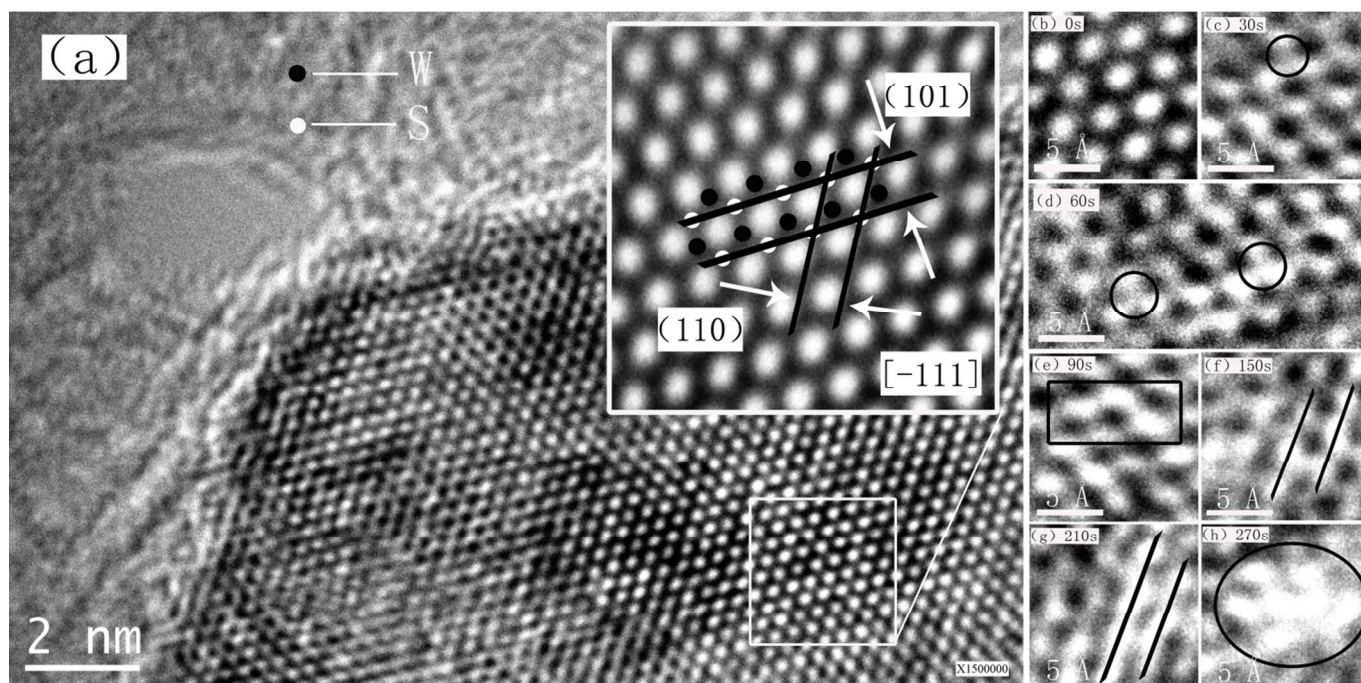
Fig. 1. (a) Pristine WS$_2$ nanosheets before irradiation. Atomic-scale structures of the changes in WS$_2$ nanosheets after electron irradiation at 100 keV for durations of (b) 0 s, (c) 30 s, (d) 60 s, (e) 90 s, (f) 150 s, (g) 210 s and (h) 270 s.

To know the impacts of irradiation, the change of atom-scale structure after irradiation are investigated by HRTEM and a series of images with various exposure time under electron acceleration voltage 100 kV are shown in Fig. 1. For the pristine WS$_2$ nanosheets, before irradiation (Fig. 1a), the ordered atomic structure where the tungsten (black dots) and sulfur atoms (white dots) aligned had a hexagonal structure in the WS$_2$ unit. According to the contrast between tungsten and sulfur, their sites can be confirmed. Fig. 1b-1h shows the changes of defect with different irradiation times. Compare the atomic structure of nanosheets to that before irradiation (Fig. 1b), a vacancy was produced when a sulfur atom was sputtered from the surface of the WS$_2$ nanosheets after 30 s of irradiation

(Fig. 1c). When the irradiation time was increased to 60 s, a clear void (the right circle in Fig. 1d) emerged because the top and bottom sulfur atoms had both been knocked out of the nanosheets. New vacancies were generated with an increasing irradiation time, leading to an increase in the vacancy concentration, as well as the conversion of the triangular vacancy clusters (Fig. 1e) into linear defects (Fig. 1f and 1g). The evolution of these defects also can be found in the MoS$_2$ nanosheets studied by Hannu-Pekka et al.[24] After prolonged exposure to the electron beam (Fig. 1h), a large hole formed in the area where the tungsten and sulfur atoms had been sputtered from.
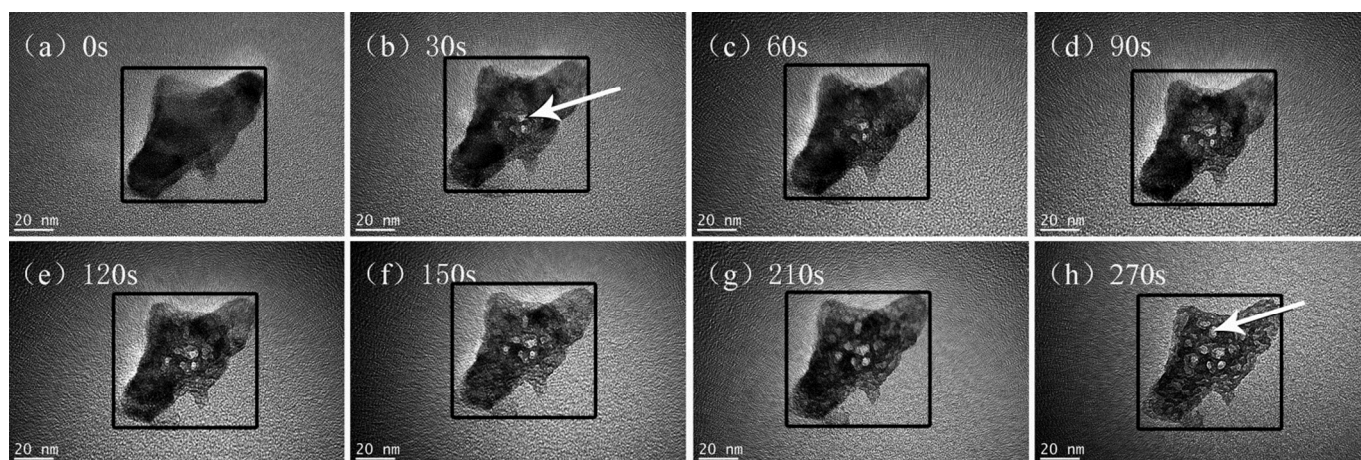
Fig. 2. Evolution of the morphology of the WS$_2$ nanosheets after 100 kV of electron irradiation, for different irradiation times.

The evolution of the morphology of the WS$_2$ nanosheets after 100 keV of electron irradiation is shown in Fig. 2 as a function of the irradiation time. Upon comparing the eight images, only some holes (the arrows shown in Fig. 2) appeared in the

nanosheets and they shrank slightly before 150 s of irradiation (Fig. 2a-2f). In contrast, additional holes and more shrinkage were observed at 210 s (Fig. 2g) and 270 s (Fig. 2h) of electron
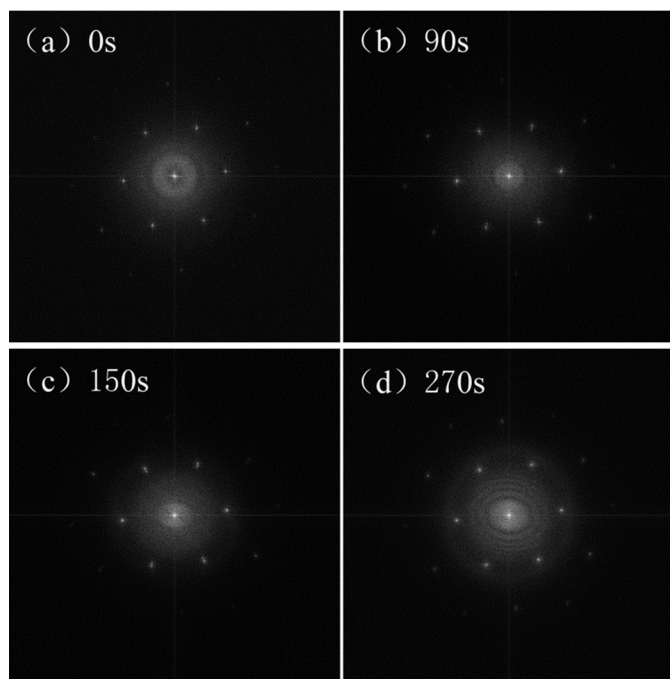
Fig. 3. Fast Fourier transformation patterns of WS_2 nanosheets after 100 keV of electron irradiation.

irradiation. This indicates that a 100 keV electron beam focused on a WS_2 nanosheets led to the generation of holes and caused the morphology to shrink slightly. To further study the structural changes, Fig. 3 shows some of the corresponding fast Fourier transformation (FFT) patterns for the morphologies of the WS_2 nanosheets shown in Fig. 2. The position and shape of the diffraction pattern did not change, but the intensities of diffraction spots became weaker. The new diffraction rings in Fig. 3d were from the amorphous carbon on the Cu grid where holes formed. This indicates that the 100 keV electron beams only knocked out some of the atoms and had little effect on the arrangement of the remaing atoms. This further demonstrates that the nanosheets hardly changed and still maintained its original crystal structure under electron irradiation of 100 keV.

The 120 keV electron beams were also used to irradiate the WS_2 nanosheets. The morphological changes of the nanosheets at different irradiation times are shown in Fig. 4. After only 30 s, many holes (the arrow in Fig. 4b) were formed on the surfaces of the WS_2 nanosheets. With an increasing irradiation time, shrinkage of the nanosheets was still observed, but some of the holes disappeared. In comparison with the WS_2 nanosheets under electron irradiation of 100 keV, the nanosheets were destroyed more easily with a 120 keV electron beam. This could be because there was enough energy to allow the remaining atoms to rearrange. To provide more evidence of the crystal structure in the nanosheets, Fig. 5 shows the FFT patterns of the nanosheets morphological under electron irradiation of 120 keV for different irradiation times. Fig. 5a shows the diffraction spots for WS_2 and the diffraction
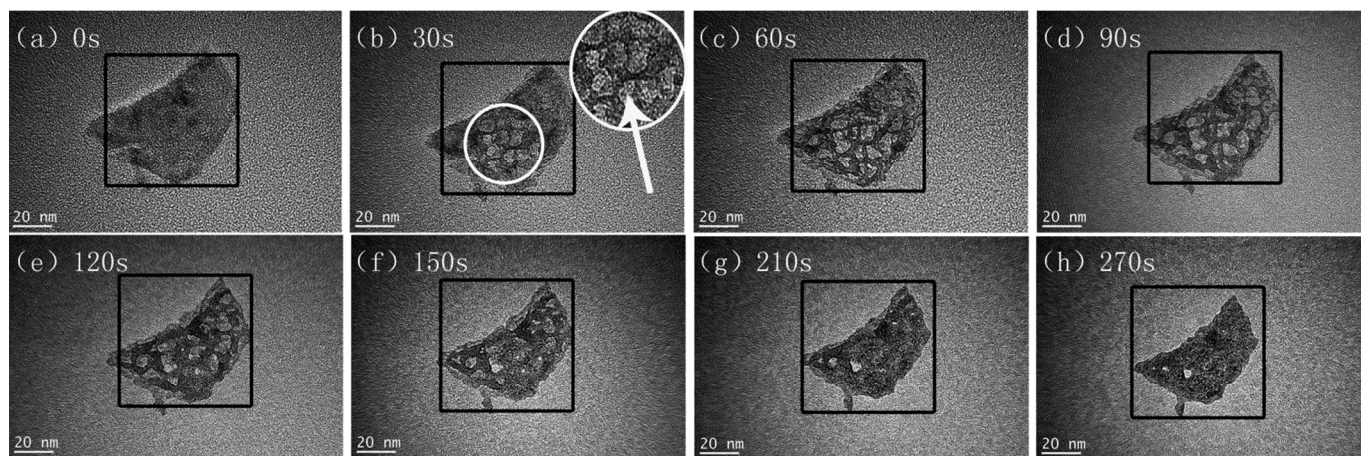
Fig. 4. Series of images showing the changes in WS_2 nanosheets after 120 keV of electron irradiation, for different irradiation times.

rings for carbon. After irradiation for 90 s, the intensities of the diffraction spots became weaker, indicating that some of the tungsten and sulfur atoms had been sputtered away, while the other atoms remained. A similar phenomenon was observed after 270 s of electron irradiation with energy of 100 keV. However, changes in the crystal structure did not occur. After 150 s of irradiation (Fig. 5d), diffraction rings for the polycrystalline structure of tungsten appeared. This demonstrates that the remaining atoms continued to rearrange, transforming the crystal structure of WS_2 into the polycrystalline structure of tungsten. In general, the structural evolutions of the WS_2 nanosheets after 120 keV of electron irradiation was not the same as that after 100 keV of electron irradiation.

As shown in Fig. 6, under electron irradiation of 200 keV there are obvious and quick changes in the morphological of the WS_2 nanosheets for different irradiation times. Fig. 6b shows that the morphology changed significantly in a short time, where some areas of the nanosheets were broken and the volume contracted as a result of the higher electron energy, which caused the atoms to move quicker after only 30 s of irradiation. With an increasing irradiation time, the nanosheets were damaged and they shrank more than those under electron irradiations of 100 and 120 keV. From the morphological changes, it was found that holes formed and shrinkage occurred almost simultaneously, which is different from what occured with low electron energies. This indicates that higher electron

energies, made it easier to sputter the atoms and their motion became quicker.

The interaction between the electron beams and the WS_2 nanosheets was different for varying irradiation energies (see

Figs. 2, 4 and 6) and the tungsten and sulfur atoms in the WS_2 nanosheets had different behaviors during the irradiation process. The atoms were activated and tended to be sputtered from the nanosheets, leaving vacancies in the WS_2 crystal
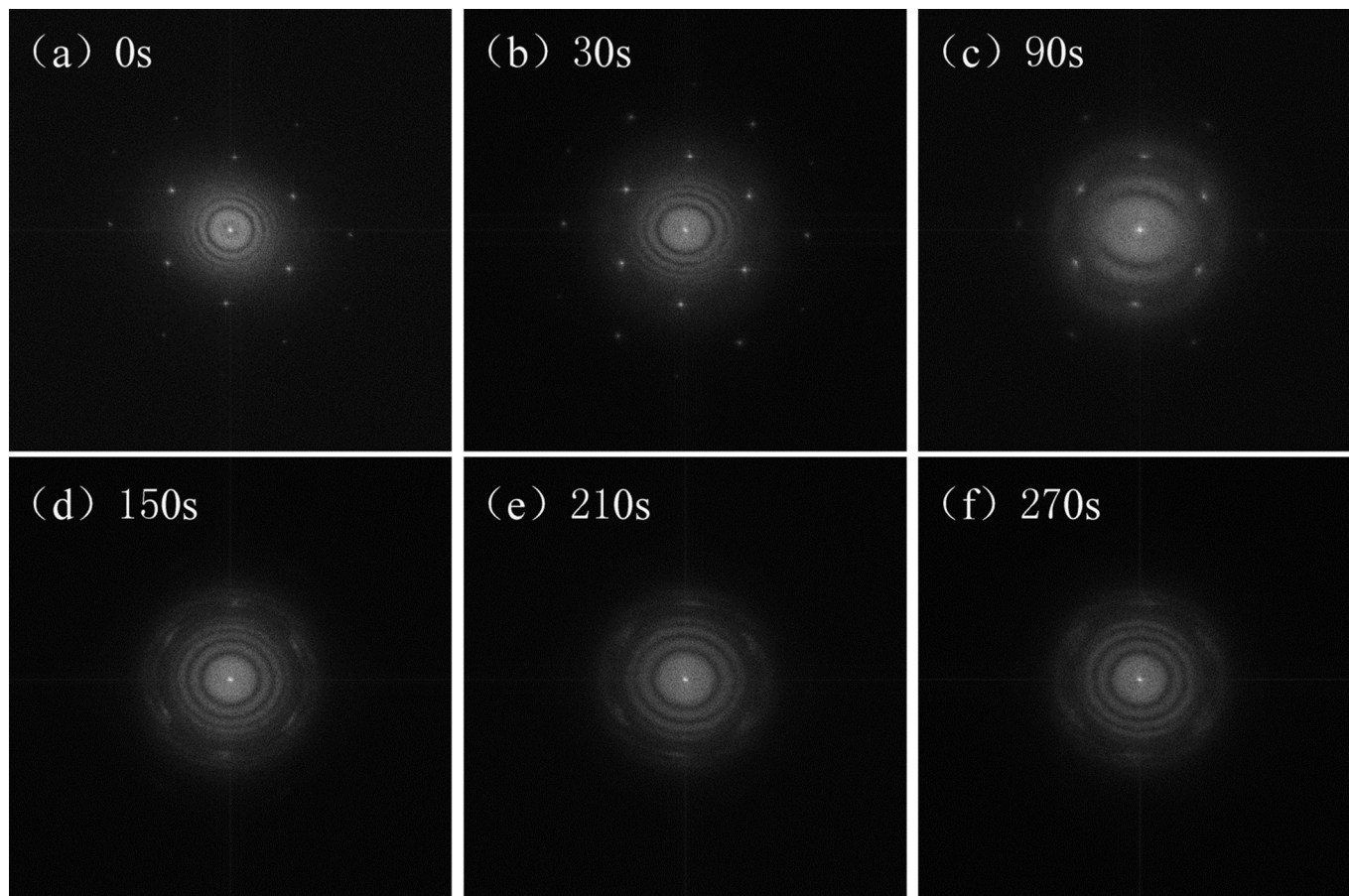
Fig. 5. Fast Fourier transformation patterns of WS_2 nanosheets after 120 keV of electron irradiation.

lattice. The remaining atoms rearranged to form a new structure. At the low irradiation energy of 100 keV, the generation of holes and the shrinkage of the nanosheets were moderate. However, there were two distinct stages under electron irradiation of 120 keV. The holes were mainly produced at the start of the 90-s cycle and as the irradiation time increased the lattice shrank and the holes disappeared. When the electron energy reached 200 keV, there was no clear boundary between the two stages, but the nanosheets shrank significantly.

The corresponding FFT patterns are shown in Fig. 7, which demonstrate the structural variations in the structure of the nanosheets. In Fig. 7a, the diffraction rings represent carbon and the hexagonally-arranged diffraction spots correspond to the WS_2 lattice plane. These spots become dim after 30 s of irradiation (Fig. 7b), revealing the changes in the structure of the nanosheets and the production of vacancies in the WS_2 nanosheets. With an increasing irradiation time, the diffraction spots became blurry, indicating that the crystal structure of nanosheets was completely damaged (Fig. 7c). New polycrystalline diffraction rings for tungsten emerged (Fig. 7d, 7e and 7f), implying that the remaining tungsten atoms had re-aligned. The crystal structure evolution derived from the FFT

images (Figs. 3, 5 and 7) is in good agreement with the changes in the morphology.

In the HRTEM measurements, the radiation damage can be divided into two categories. The first one is knock-on damage, which is related to the displacement of atoms through direct collisions between the energetic and target atoms. The second is from excitation of the electronic system of the target.[26] Based on the above observations, the dominant radiation damage mechanism in the WS_2 nanosheets was knock-on damage, which is similar to the MoS_2 samples under electron irradiation, studied by Hannu-Pekka Komsa *et al.*[27] Irradiating the WS_2 nanosheets followed gradual morphological and structural evolution processes. At first, sulfur atoms were sputtered away and vacancies were generated in the nanosheets, then linear defects formed. With increasing irradiation time, when the sulfur atoms that surrounded a tungsten atom had been sputtered away, the tungsten atom had no W-S bonds and had enough energy to be sputtered, leaving a new vacancy in the WS_2 crystal lattice. If the remaining tungsten atoms did not have enough energy to be sputtered away, they migrated toward each other and rearranged to form atomic-scale tungsten crystal.
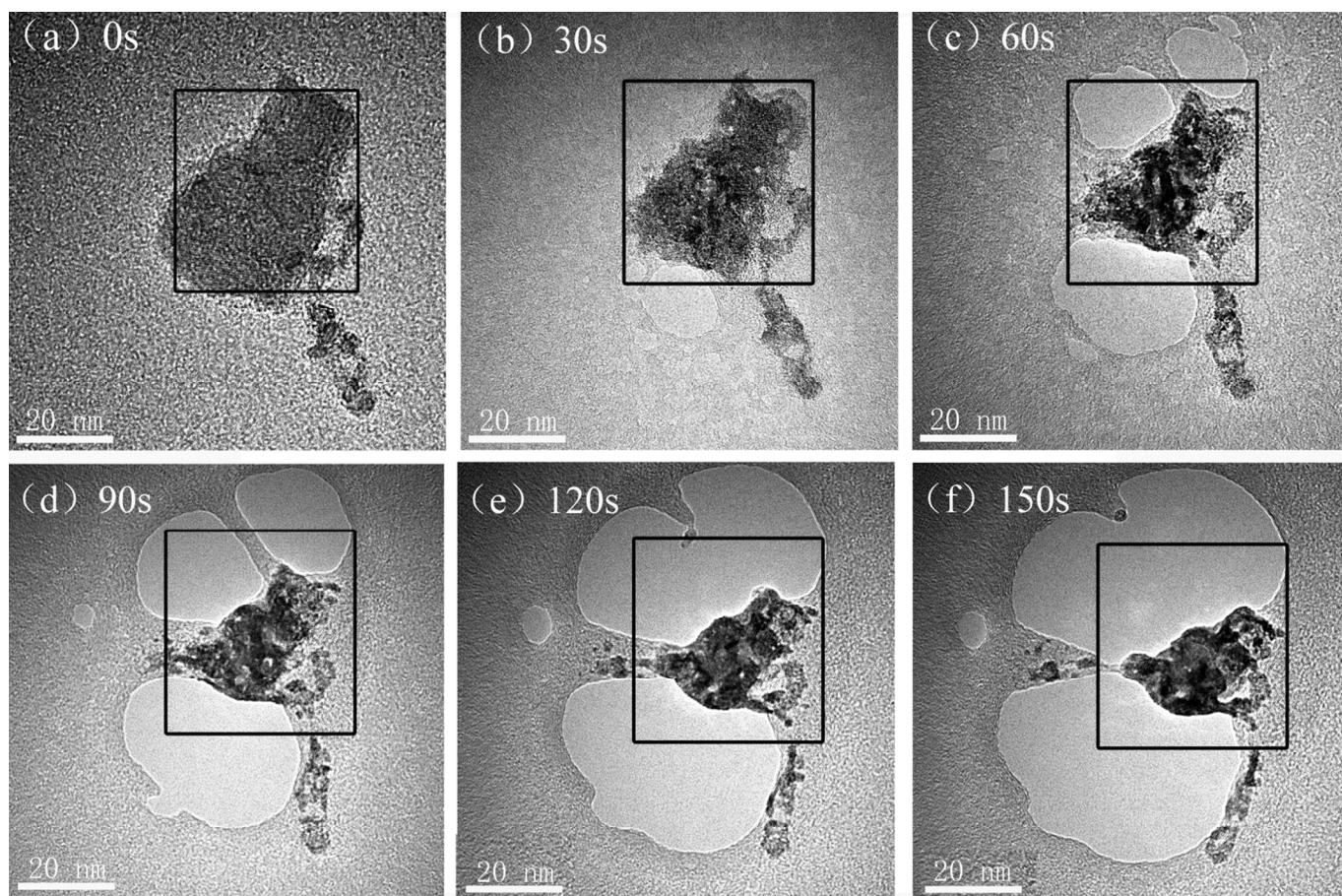
Fig. 6. Evolution of the morphology of the WS_2 nanosheets, after 200 keV of electron irradiation.

To understand the kinetics of WS_2 sputtering, the interactions between the electron collisions and atoms were investigated. First, electron elastic collisions with the WS_2 nanosheets transferred part of their energy to the targeted tungsten and sulfur atoms. The maximum amount of energy transferred to the target atoms can be calculated using[28]

$$E_{max} = \frac{2E_e \left(E_e + 2m_e C^2 \right)}{MC^2} \quad (1)$$

where E_e is the electron energy, m_e and M are the electron and target atom masses respectively, and C is the speed of light. According to Eq. 1, E_{max} decreases as the mass of the target atoms increases and is proportional to the incident electron energy, in other words, the displacement of a heavy tungsten atom requires a higher incident electron energy than that of a light sulfur atom. A higher incident electron energy facilitates the easier displacement of atoms.

If E_{max} exceeds the displacement threshold energy (T_d) of an atom, a large angle scattering can permanently displace atoms from their lattice sites and change the crystal structure. When $E_{max} = T_d$, the electron energy is the minimum incident energy of a target atom sputtered. And because of $m_e c^2$=511 keV >> T_d and $M/m_e \approx 1823$ A >> 1, where A is the atomic mass number of an atom. The minimum incident energy (E_e^{min}) is[29]

$$E_e^{min} = (511 keV) \left\{ [1 + A T_d / (561 eV)]^{1/2} - 1 \right\} \quad (2)$$

According to Eq. (2), E_e^{min} increases with an increasing displacement threshold energy and atomic number.

For electron-induced sputtering, T_d is the sublimation energy E_{sub}.[27,29] The calculated minimum electron energies for sulfur and tungsten are listed in Table 1. The minimum electron energy for the sulfur is lower than 100 keV. In contrast, the minimum electron energy for tungsten is higher than 100 keV. Therefore, the sulfur atoms were easier to sputter than the tungsten atoms, which is consistent with the experimental results. Because of the higher displacement threshold of the tungsten atoms compared with the sulfur atoms and the tendency of the tungsten atoms to form metallic clusters, the tungsten atoms aggregated

Journal Name

ARTICLE
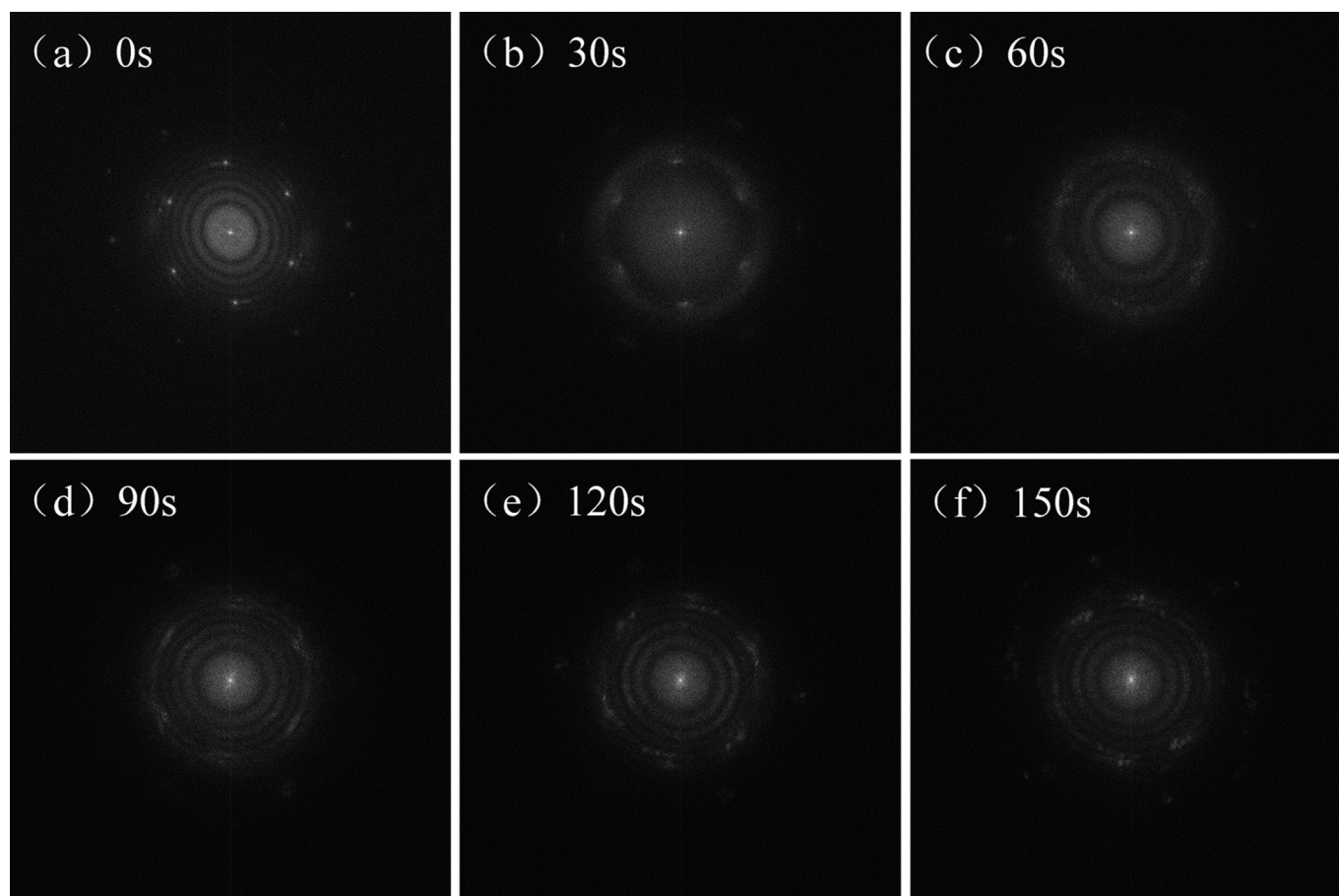
Fig. 7. Fast Fourier transformation patterns of the images for the duration of (a) 0 s, (b) 30 s, (c) 60 s, (d) 90 s, (e) 120 s, and (f) 150 s.

Table 1. The minimum electron energies evaluated for displacement energies of E_{sub}.

Element symbol	Atomic wt.	E_{sub}(eV)	E_e^{min} (keV) for $T_d = E_{sub}$
S	32.1	6.9	93
W	183.9	8.92	501

at the edges of the damaged areas, while the sulfur atoms were simply sputtered away.[30] When the S atoms surrounding a tungsten atom had all been sputtered away, the W-S chemical bonds were broken and the WS_2 lattice networks became very unstable. This decreased the displacement threshold energy of the tungsten atoms, allowing the isolated tungsten atoms to be sputtered. It can be concluded that the sulfur atoms were sputtered much easier than tungsten atoms under the same irradiation conditions and higher electron energies caused the atoms to be sputtered faster.

Table 2. The S/W ratios under different electron energy with different irradiation time.

Irradiation times (s)	0	30	60	90	120	150	210	270
The ratio (S/W) at 100 keV	1.54	1.27	1.06	1.00	0.82	0.64	0.61	0.60
The ratio (S/W) at 120 keV	1.47	1.12	0.92	0.68	0.62	0.52	0.43	0.37
The ratio (S/W) at 200 keV	1.5	0.65	0.17	0.12	0.06	0.03	-	-

Journal Name

RSC**Publishing**

ARTICLE

The energy dispersive spectra (EDS) of WS_2 nanosheets irradiated by different electron energy beams were also examined. Table 2 shows the S/W ratio under different electron energies for different irradiation times. The corresponding curves are shown in Fig. 8.The initial S/W ratio was about 1.5. It was less than 2 because the WS_2 nanosheets were not fully
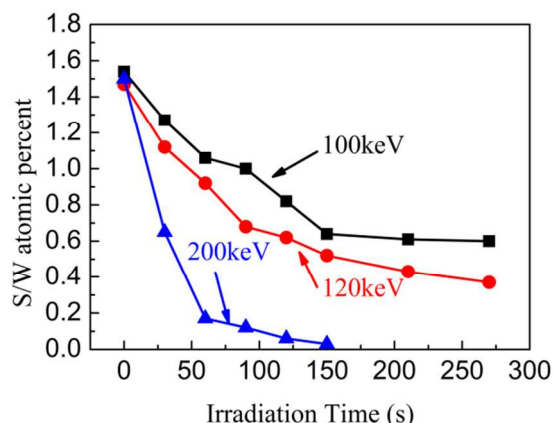
Fig. 8. The S/W ratio curves under different electron energies for different irradiation times.

intact and some defects were introduced during the preparation process.[31] The decline of every curve indicates the faster reduction of the sulfur atoms than that of the tungsten atoms, which also occurred in WS2 nanotubes, demonstrated by Kewang Ding et al.[32] Under electron irradiation of 200 keV, the sulfur atoms disappeared. However, there was a surplus of tungsten atoms at 150 s and the declining rates of the S/W ratio was quicker than the other energies, indicating that the sulfur atoms were sputtered quickly under high electron energies. The EDS results are consistent with the morphological and structural evolution (Figs. 6 and 7). The S/W ratio at 100 keV decreased initially, becoming stable after 150 s of irradiation. This was because the electron energy was close to 93 keV and at this energy it is not easy to sputter the all of sulfur atoms in an intact WS_2 lattice. Compared with 120 keV, after 150 s the S/W ratio still had a slow decline, which indicates that the process of sputtering sulfur atoms under irradiation of 120 keV takes longer and is more serious than that under irradiation of 100 keV. These changes are consistent with the previous evolution of the morphology (Figs. 2 and 4) and also demonstrate that our inference is reasonable. In general, the damage to the WS_2 nanosheets became worse with increasing electron energy and was proportional to the irradiation time.

Conclusions

In summary, this study shows that some of the sulfur atoms in WS_2 nanosheets could be sputtered to form vacancies under electron irradiation of 100 keV and these vacancies generated linear defects with an increasing irradiation time. Once the sulfur atoms that surrounded a tungsten atom are sputtered away, the remaining tungsten atom could be sputtered. The remaining atoms were attracted to each other and moved, making a smaller hole, when they had enough energy. This shows that some parts of the nanosheets shrunk on the macro level and rearranged to form the polycrystalline structure of tungsten. What is more, it can be concluded that there were two stages in the irradiation process. One was that holes formed, and the other was that the lattice shrank, which was clearly observed at 120 keV of electron irradiation. In addition, the nanosheets became more damaged with increasing electron energy and this damage was proportional to the irradiation time. On the whole, the WS_2 nanosheets could be destroyed by electron beams with energies greater than 100 keV and the sulfur atoms were easily sputtered than the tungsten atoms. As the nanosheets had different changes with different electron energies, the electron energy could be controlled to obtain the desired structure.

Notes and references

*The corresponding author is Yi Feng. E-mail: fyhfut@163.com.

1   H. Zhang, X.-B. Li and L.-M. Liu, *J. Appl. Phys.*, 2013, **114**, 093710.
2   Y. Ma, Y. Dai, M. Guo, C. Niu, Y. Zhu and B. Huang, *ACS nano*, 2012, **6**, 1695-1701.
3   K. F. Mak, C. Lee, J. Hone, J. Shan and T. F. Heinz, *Phys. Rev. Lett.*, 2010, **105**, 136805.
4   G. Cunningham, M. Lotya, C. S. Cucinotta, S. Sanvito, S. D. Bergin, R. Menzel, M. S. Shaffer and J. N. Coleman, *ACS nano*, 2012, **6**, 3468-3480.
5   P. May, U. Khan, J. M. Hughes and J. N. Coleman, *The Journal of Physical Chemistry C*, 2012, **116**, 11393-11400.
6   R. J. Smith, P. J. King, M. Lotya, C. Wirtz, U. Khan, S. De, A. O'Neill, G. S. Duesberg, J. C. Grunlan and G. Moriarty, *Advanced Materials*, 2011, **23**, 3944-3948.
7   A. S. Golub, Y. V. Zubavichus, Y. L. Slovokhotov and Y. N. Novikov, *Russ. Chem. Rev+*, 2003, **72**, 123-141.
8   Z. Zeng, T. Sun, J. Zhu, X. Huang, Z. Yin, G. Lu, Z. Fan, Q. Yan, H. H. Hng and H. Zhang, *Angewandte Chemie International Edition*, 2012, **51**, 9052-9056.

9   Z. Zeng, Z. Yin, X. Huang, H. Li, Q. He, G. Lu, F. Boey and H. Zhang, *Angewandte Chemie International Edition*, 2011, **50**, 11093-11097.

10   B. Liu, L. Chen, G. Liu, A. N. Abbas, M. Fathi and C. Zhou, *ACS nano*, 2014.

11   B. Radisavljevic, A. Radenovic, J. Brivio, V. Giacometti and A. Kis, *Nat. Nanotechnol*, 2011, **6**, 147-150.

12   K. Chang and W. Chen, *ACS nano*, 2011, **5**, 4720-4728.

13   L. David, R. Bhandavat and G. Singh, *ACS nano*, 2014.

14   Y. Liang, R. Feng, S. Yang, H. Ma, J. Liang and J. Chen, *Advanced Materials*, 2011, **23**, 640-643.

15   H. R. Gutiérrez, N. Perea-López, A. L. Elías, A. Berkdemir, B. Wang, R. Lv, F. López-Urías, V. H. Crespi, H. Terrones and M. Terrones, *Nano Lett.*, 2012, **13**, 3447-3454.

16   H. S. Lee, S.-W. Min, Y.-G. Chang, M. K. Park, T. Nam, H. Kim, J. H. Kim, S. Ryu and S. Im, *Nano Lett.*, 2012, **12**, 3695-3700.

17   Z. Yin, H. Li, H. Li, L. Jiang, Y. Shi, Y. Sun, G. Lu, Q. Zhang, X. Chen and H. Zhang, *ACS nano*, 2011, **6**, 74-80.

18   R. Bhandavat, L. David and G. Singh, *The Journal of Physical Chemistry Letters*, 2012, **3**, 1523-1530.

19   J. N. Coleman, M. Lotya, A. O'Neill, S. D. Bergin, P. J. King, U. Khan, K. Young, A. Gaucher, S. De and R. J. Smith, *Science*, 2011, **331**, 568-571.

20   L. P. Hansen, Q. M. Ramasse, C. Kisielowski, M. Brorson, E. Johnson, H. Topsoe and S. Helveg, *Angewandte Chemie*, 2011, **50**, 10153-10156.

21   Y. Shi, W. Zhou, A.-Y. Lu, W. Fang, Y.-H. Lee, A. L. Hsu, S. M. Kim, K. K. Kim, H. Y. Yang and L.-J. Li, *Nano Lett.*, 2012, **12**, 2784-2791.

22   A. Santana, A. Zobelli, J. Kotakoski, A. Chuvilin and E. Bichoutskaia, *Phys. Rev. B*, 2013, **87**, 094110.

23   J. Brivio, D. T. Alexander and A. Kis, *Nano Lett*, 2011, **11**, 5148-5153.

24   H.-P. Komsa, S. Kurasch, O. Lehtinen, U. Kaiser and A. V. Krasheninnikov, *Phys. Rev. B*, 2013, **88**.

25   X. Zhu, L. Li, S. Huang, Z. Wang, G. Q. M. Lu, C. Sun and L. Wang, *Carbon*, 2011, **49**, 3120-3124.

26   G. Algara-Siller, S. Kurasch, M. Sedighi, O. Lehtinen and U. Kaiser, *Applied Physics Letters*, 2013, **103**, 203107.

27   H.-P. Komsa, J. Kotakoski, S. Kurasch, O. Lehtinen, U. Kaiser and A. V. Krasheninnikov, *Phys. Rev. Lett.*, 2012, **109**.

28   B. Li, Y. Feng, K.-w. Ding, G. Qian, X.-b. Zhang and Y.-f. Liu, *Transactions of Nonferrous Metals Society of China*, 2014, **24**, 764-769.

29   R. F. Egerton, R. McLeod, F. Wang and M. Malac, *Ultramicroscopy*, 2010, **110**, 991-997.

30   R. Zan, Q. M. Ramasse, R. Jalil, T. Georgiou, U. Bangert and K. S. Novoselov, *ACS Nano*, 2013, **7**, 10167-10174.

31   Z. Liu, K. Suenaga, Z. Wang, Z. Shi, E. Okunishi and S. Iijima, *Nat. Commun.*, 2011, **2**, 213.

32   K. Ding, Y. Feng, S. Huang, B. Li, Y. Wang, H. Liu and G. Qian, *Nanotechnology*, 2012, **23**, 415703.